Histochem Cell Biol (2002) 118:459–472
DOI 10.1007/s00418-002-0469-0

ORIGINAL PAPER

Christoph Radcke · Thomas Stroh
Florian Dworkowski · Rüdiger W. Veh

Specific visualization of precipitated cerium by energy-filtered transmission electron microscopy for detection of alkaline phosphatase in immunoenzymatic double labeling of tyrosine hydroxylase and serotonin in the rat olfactory bulb

Accepted: 18 October 2002 / Published online: 26 November 2002

Abstract To understand in detail the functional morphology of neuronal circuits it is important to identify at the ultrastructural level the incoming axon, its target neuron, and members of the signaling cascades involved. This, however, represents a formidable task, requiring highly sophisticated electron microscopic multiple-labeling techniques. To extend available double-labeling procedures such as combinations of immunogold and peroxidase methods, an additional, gold- and peroxidase-independent procedure would represent a considerable advantage. The present investigation therefore aimed to use alkaline phosphatase as the immunoenzymatic label at the electron microscopic level via cerium phosphate precipitates. To our surprise we found that available techniques, which are well established for the visualization of endogenous enzymes in sections from various tissues, are not suitable for application to immunocytochemistry. Careful characterization of the individual reaction conditions, however, resulted in an optimized procedure with largely increased sensitivity. The novel technique yields cerium-containing precipitates which are massive enough to allow the detection of the immunoenzymatic reaction product in the electron microscope. Using the rat olfactory bulb as the model system we showed further that our technique allows the combination with the peroxidase/diaminobenzidine system for ultrastructural double labeling. For this purpose, the alkaline phosphatase product is identified by its cerium content via energy-filtered transmission electron microscopy and thereby differentiated from cerium-free peroxidase-derived precipitates. Doing so, we found that ascending serotoninergic fibers do not establish synapses with dopaminergic periglomerular cells in the rat olfactory bulb.

Keywords Preembedding · Double staining · Ultrastructure · Immunocytochemistry · ESI · EELS

Introduction

For a detailed understanding of the molecular and functional anatomy of neuronal circuits, the connections between individual neurons and the signaling cascades involved have to be known. This information can be obtained when the incoming axon, its target neuron, the transmitter, its receptor, and further partners of the transmission process, such as ion channels, G-proteins, kinases, phosphatases, or phospholipases are identified at the ultrastructural level. This, however, represents a formidable task, requiring highly sophisticated electron microscopic multiple-labeling procedures.

For double labeling at the ultrastructural level, postembedding staining with two species of differently sized gold granules is a well-established procedure (Wenzel et al. 1997). Unfortunately, visualization of many antigens depends on epitopes, which are destroyed or masked during polymerization procedures of epoxy- or acryl-based resins. This problem severely limits the scope of postembedding techniques. In contrast, preembedding procedures are quite effective when a horseradish peroxidase-based precipitate is used for visualization. Double labeling by combination with gold granules, however, with or without silver intensification, is usually compromised by penetration problems of the gold-labeled secondary antibody. For multiple labeling at the electron

This work contains part of the PhD Thesis of Christoph Radcke at the Technische Universität Berlin, Institut für Biotechnologie, Gustav-Meyer-Allee 25, 10115 Berlin, Germany

C. Radcke · T. Stroh · F. Dworkowski · R.W. Veh (✉)
Institut für Anatomie der Charité,
Universitätsklinikum der Humboldt-Universität zu Berlin,
Philippstrasse 12, 10115 Berlin, Germany
e-mail: ruediger.veh@charite.de
Tel.: +49-30-450528062, Fax: +49-30-450528912

Present address:
C. Radcke, WITA, Warthestrasse 21, 14513 Teltow, Germany

microscopic level, therefore, an additional gold- or peroxidase-independent procedure would represent a considerable advantage.

Visualization systems with alkaline phosphatase-based precipitates, as known from light microscopy, may offer a solution to this problem. These precipitates are commonly based on either the reduction of a tetrazolium salt by an indole, released from its phosphate ester by phosphatase action, or by the formation of azo dyes from diazonium salts and substituted naphthols, the latter again liberated from phosphorylated precursors by the enzyme. Unfortunately, both precipitates are soluble in alcohol, precluding embedding in epoxy or acrylic resins. Furthermore, they do not provide enough electron density for application in electron microscopy.

However, there is another procedure for the cytochemical visualization of phosphatase activity (Robinson and Karnovsky 1983; Halbhuber et al. 1992, 1994; van Noorden and Frederiks 1993). In theory, this technique should provide all the necessary properties. In the course of this procedure, inorganic phosphate is released from phosphomonoesters such as para-nitrophenyl phosphate or β-glycerophosphate and precipitates with cerium ions. The primary product, invisible cerium-(III) phosphate, is subsequently converted to the visible and less soluble cerium-(IV) hydroperoxide by oxidation with hydrogen peroxide [the cerium phosphate peroxide (CPP) technique].

Unfortunately, when combined with diaminobenzidine (DAB)/osmium tetroxide-based peroxidase immunocytochemistry, there is no possibility to distinguish the two electron-dense precipitates in the conventional electron microscope. Differentiation can be achieved, however, by element-specific visualization of cerium via energy-filtered transmission electron microscopy (EFTEM). The cerium phosphate procedure, therefore, in combination with EFTEM has the potential to add to and improve available methods for multiple labeling at the ultrastructural level.

The present study, therefore, aimed to investigate, whether the above theoretical considerations hold in reality, when it is attempted to use alkaline phosphatase as one signal system for immune electron microscopic double labeling. The rat olfactory bulb was chosen as the model system. Here, incoming olfactory axons target the dendrites of mitral and tufted cells. This interaction is controlled by dopaminergic periglomerular cells and serotoninergic input from the raphe nuclei. Presently, it is still unknown whether serotoninergic axons directly contact dopaminergic neurons. Solving this question requires simultaneous visualization of serotonin on the one side and tyrosine hydroxylase as marker for dopaminergic neurons on the other side. Both antigens do not withstand resin embedding. Pre-embedding staining with simultaneous immunoenzymatic visualization of serotonin and tyrosine hydroxylase via ultrastructural peroxidase and alkaline phosphatase cytochemistry may offer a novel possibility to solve the problem.

Materials and methods

Animals

Adult Wistar rats of both sexes were anesthetized with 0.1 mg/g body weight ketamine hydrochloride (Ketamin; Curamed Pharma, Karlsruhe, Germany), 20 µl xylazine hydrochloride (2% Rompun; BayerVital, Leverkusen, Germany), and 5 IE heparin sodium (Heparin-Natrium-25000; Ratiopharm, Ulm, Germany). Transcardial perfusion with physiological salts solution containing dextran and heparin (Longasteril; Fresenius Kabi Deutschland, Bad Homburg, Germany) was followed by fixation solution (4% paraformaldehyde, 0.05% glutaraldehyde, 0.2% picric acid in 0.1 M phosphate buffer). Brains and kidneys were rinsed with 0.1 M phosphate buffer (PB) containing 5% sucrose and dissected from the animal. Thick (1–3 mm) slices were cryoprotected overnight in 30% sucrose solution in 0.1 M PB, frozen at –60°C in hexane, and stored at –80°C until use.

Immunoenzymatic single staining for light microscopy with alkaline phosphatase as signal system

Cryosections were cut at 25 µm on a cryostat (2800 Frigocut E; Leica, Heidelberg, Germany). Freely floating sections were washed three times with phosphate-buffered saline (PBS; pH 7.4) and reacted for 15 min in 1% $NaBH_4$ (Sigma, St. Louis, Mo., USA) in PBS. Following treatment for 30 min in 0.05% phenylhydrazine (Merck, Darmstadt, Germany) and 10% normal goat serum (NGS; PAN Biotech, Aidenbach, Germany) in PBS containing 0.3% Triton X-100 (Serva, Heidelberg, Germany), they were incubated with anti-tyrosine hydroxylase (Roche Diagnostics, Mannheim, Germany) diluted 1:1,000 in antibody dilution buffer (10% NGS, 0.3% Triton X-100, 0.1% sodium azide, 0.01% thimerosal in PBS) for 36 h at 4°C. Subsequently, sections were rinsed twice (20 and 40 min) with PBS, preincubated with 0.2% bovine serum albumin (BSA; Serva) in PBS for 60 min, and transferred to biotinylated secondary antibody (biotinylated goat anti-rabbit IgG; Vector, Burlingame, Calif., USA), diluted 1:2,000 in 0.2% BSA and 0.1% sodium azide in PBS, for 16 h at 4°C. After washing with PBS and preincubation for 1 h with 0.2% BSA in PBS, they were incubated overnight at room temperature in alkaline phosphatase-labeled streptavidin (Life Technologies, Eggenstein, Germany), diluted 1:1,000 in 0.2% BSA in PBS, and visualized as described below (see visualization reactions). Control experiments were performed with antigen-absorbed primary antibodies and by omission of primary antibodies.

Immunoenzymatic single staining for electron microscopy with alkaline phosphatase as signal system

For electron microscopy, thick sections (40 µm) were cut on a vibratome 3000 (Ted Pella, Reddin, Calif., USA) and treated as described except for the use of Triton X-100, which was only present at 0.1% in the preincubation step prior to the primary antibody incubation.

Immunoenzymatic double staining for light and electron microscopy

Double staining of cryosections or vibratome sections was carried out using the same treatments as above. Simultaneous incubation with mouse anti-tyrosine hydroxylase diluted 1:1,000 and rabbit anti-serotonin diluted 1:100 (Behringer et al. 1991) was followed by secondary antibodies (biotinylated goat anti-rabbit IgG and alkaline phosphatase-labeled horse anti-mouse IgG; both from Vector) at final dilutions of 1:2,000 and 1:500, respectively. ABC complex (Vector) was diluted 1:1,000 in 0.2% BSA in PBS and the secondary alkaline phosphatase-labeled antibody 1:500 in the

same solution. Incubation in ABC complex/alkaline phosphatase secondary antibody solution for 18 h at 4°C was followed by three washings (10, 20, and 30 min) and the immunoenzymatic visualization reactions.

In addition to the controls outlined for single labeling, sections were incubated with either of the primary antibodies alone. They were then developed as described below using both signal systems to control for crossreactivities of the secondary antibodies.

Immunoenzymatic visualization reactions for light microscopy

Visualization of alkaline phosphatase with the bromochloroindolyl phosphate/nitro blue tetrazolium (BCIP/NBT) method (McGadey 1970) or the conventional CPP technique (Halbhuber et al. 1992), and peroxidase (Behringer et al. 1991) with DAB were carried out according to published protocols.

Characterization and optimization of individual reaction parameters of the conventional cerium technique for alkaline phosphatase visualization

For the elaboration of optimized CPP reaction conditions for immunocytochemistry, alkaline phosphatase activity was determined colorimetrically at 405 nm following the cleavage of para-nitrophenyl phosphate to nitrophenol. The experiments were performed with 50 mU alkaline phosphatase-labeled streptavidin and varying reaction parameters such as buffer systems (glycine, glycine-tricine, tricine, tricine-diethanolamine), buffer concentrations (50 and 100 mM each), and pH values (8.0, 8.5, 9.0, 9.5, 10.0, 10.5, 11.0). Several substrates such as para-nitrophenyl phosphate, β-glycerophosphate, and ethanolamine phosphate were evaluated. Finally, the phosphatase was offered different cerium concentrations (0, 3, 6, 10 mM), with and without $MgSO_4$, CO_2, and sucrose. Individual reactions were carried out in duplicate in microtiter plates and repeated at least three times. The increase of extinction over time was measured in a conventional ELISA reader (Dynatech MR 5000, Denkendorf, Germany).

Based on the biochemically optimized conditions the visualization of alkaline phosphatase via cerium phosphate was optimized in tissue sections. After enzyme incubation for 30–600 min at 37°C, the primary product was oxidized with varying concentrations of H_2O_2 (0.2%, 0.4%, 0.8%) and enhanced with DAB (0.2, 0.5, 0.8 mg/ml), using different enhancement buffers (50 mM TRIS, 100 mM acetate). Finally optimized conditions (oCPP technique) are given below.

Visualization of alkaline phosphatase activity with the novel oCPP technique for light microscopy

Subsequent to incubation with alkaline phosphatase-labeled secondary antibodies or streptavidin, the sections are washed five times for 10 min in 50 mM tricine buffer (pH 10) and preincubated for 15 min in cerium incubation buffer [50 mM tricine, 50 mM diethanolamine, 3 mM cerium-(III) chloride heptahydrate (Fluka Chemie, Buchs, Switzerland), 3.9 mM $MgSO_4$, 30% sucrose, and 2 mM levamisole] at pH 10. The reaction is started by adding 1 mM para-nitrophenyl phosphate and stopped after 100 min at 37°C by washing with 50 mM tricine buffer. After another three brief washes, the cerium precipitate is stabilized and visualized by oxidation with 0.2% H_2O_2 in 50 mM tricine buffer for 5 min. After four short rinses in 50 mM tricine buffer the reaction product is enhanced with 0.5 mg/ml DAB and 2% ammonium nickel sulfate in 100 mM sodium acetate buffer at pH 5.3. After three final washes in PBS the sections are mounted onto chrome alum/gelatin-coated slides, dehydrated via an ascending series of ethanols, cleared in xylene, and coverslipped with Entellan. Control experiments are performed with antigen-absorbed primary antibodies and by omission of primary antibodies.

In double-staining experiments peroxidase activity was revealed first. Subsequently, the sections were reacted for visualization of alkaline phosphatase via the oCPP technique as described above.

In addition to the controls outlined for single labeling, sections were incubated with either of the primary antibodies alone. They were then developed as described above using both signal systems to control for crossreactivities of the secondary antibodies.

Visualization of alkaline phosphatase activity with the novel oCPP technique for electron microscopy

For electron microscopy, the CPP product was not enhanced with DAB. Subsequent to the stabilization of the reaction product with H_2O_2, the sections were postfixed with 1% aqueous OsO_4 for 30 min, dehydrated, and flat-embedded in Araldite. Ultrathin sections (80 nm) were cut on a Leica Ultracut UCT ultratome using a Diatome knife and counterstained with saturated uranyl acetate and lead citrate (Reynolds 1963). They were analyzed using conventional TEM and EFTEM, electron energy loss spectroscopy (EELS), and electron spectroscopic imaging (ESI) on a LEO 912 Omega electron microscope, equipped with a slow scan high speed camera (Proscan, Scheuring, Germany) and the SIS3.0 software (Soft Imaging System, Münster, Germany).

Electron microscopic identification of the oCPP product by EFTEM

For ESI analysis of cerium, the three-window power law method was used at the M4/M5 ionization edge with an energy window of 30 eV. To obtain unequivocal localization of the tyrosine hydroxylase immunoreactivity, the oCPP product was visualized with the aid of ESI. For this purpose, electron micrographs were taken at an energy loss of 792 and 863 eV and used to extrapolate the background intensities of every pixel at the M4 edge (see Discussion). These intensities were subtracted from the M4 edge micrograph at 887 eV, resulting in the specific cerium localization. The sequence was completed by a so-called high-contrast image, obtained at 250 eV in front of the carbon K-edge. Finally, the specific cerium distribution was superimposed on top of the inverted high-contrast image. The final photograph displays the ultrastructural distribution of the cerium-containing oCPP product with concomitant high morphological detail of the surrounding area.

Final protocol for the simultaneous immunoenzymatic visualization of alkaline phosphatase and peroxidase activities

Solutions

1. Preincubation buffer 1: dissolve 3 mg DAB in 1 ml H_2O, 1 ml TRIS stock, 8 ml H_2O and add 100 µl imidazole stock.
2. Incubation buffer 1: 0.5 ml preincubation buffer 1 and start reaction by addition of 25 µl H_2O_2.
3. TRIS stock: dissolve 12.2 g TRIS-(hydroxymethyl)-aminomethane in 200 ml H_2O and adjust pH value to 7.6.
4. Imidazole stock: dissolve 681 mg imidazole in 10 ml H_2O and adjust pH value to 7.6.
5. Tricine buffer: 8.99 g tricine (50 mM) in 1,000 ml boiled and precooled H_2O.
6. Preincubation buffer 2: 0.27 g tricine (50 mM), 10.8 g sucrose (30%), 29 mg $MgSO_4$ (3.9 mM) in 28 ml boiled and precooled H_2O (mix carefully). Add 0.158 g diethanolamine (50 mM), adjust pH value to 10 with 1 N NaOH, and fill up to 30 ml.
7. Reaction buffer 2: mix 10 ml preincubation buffer carefully with 11 mg $CeCl_3$ (3 mM) and 100 µl levamisole stock.
8. Para-nitrophenyl phosphate stock: 45.7 mg para-nitrophenyl phosphate (100 mM) in 1 ml H_2O.
9. Levamisole stock: 0.482 g levamisole (200 mM) in 10 ml H_2O.
10. Diaminobenzidine stock: 50 mg DAB (50 mg/ml) in 1 ml H_2O.

11. Conversion buffer (cerium oxidation): 0.2% H_2O_2 diluted in tricine buffer.
12. Diaminobenzidine enhancement buffer: 81.6 mg sodium acetate (0.1 M) adding 2 ml H_2O, 4 ml 3% ammonium nickel sulfate (2%), adjust pH value to 5.3, and 60 µl DAB stock (0.5 mg/ml).

Procedure

1. Incubate with antibodies and signal systems as described in Materials and methods.
2. Rinse three times for 20 min with PBS.
3. Preincubate for 15 min with preincubation buffer 1.
4. Change for incubation buffer 1 and start peroxidase reaction by adding 25 µl 0.3% H_2O_2 for 10 min.
5. Rinse two times for 5 min with PBS and incubate for 10 min in PBS with 0.1% NaN_3.
6. Rinse three times for 20 min with tricine buffer.
7. Preincubate for 30 min in preincubation buffer 2.
8. Change solution for 500 µl reaction buffer 2 and start reaction by adding 5 µl para-nitrophenyl phosphate stock (reaction temperature 37°C) for about 100 min.
9. Rinse four times for 5 min with tricine buffer.
10. Oxidize cerium-(III) to cerium-(IV) via conversion buffer (yields a yellow precipitate useable for electron microscopy or light microscopic double staining procedures).
11. Dehydrate with ascending series of ethanol and embed flat sections in Araldite.

Analysis of serotonin-positive axon terminals

Serotonin-positive axons were analyzed for synaptic terminals after single staining with peroxidase or double staining with the above alkaline phosphatase/peroxidase sequence. After selecting appropriate fields in adjacent semithin sections, serotonin containing axons and terminals were identified by the dark DAB/osmium staining in the single technique and the absence of cerium in dark structures in the double staining procedure.

Results

An alkaline phosphatase technique, which is suitable for electron microscopy, must provide an alcohol-insoluble and electron-dense reaction product. Visualization of alkaline phosphatase activity via the conventional cerium phosphate procedure (Halbhuber et al. 1992; von Noorden and Frederiks 1993) yields such a precipitate. Subsequent treatment with peroxide further decreases the solubility of the product and is used to polymerize DAB for inspection at the light microscopic level. As an example, the brush border of rat kidney proximal tubules is a well-known source of high endogenous alkaline phosphatase activity. It can be visualized either with the widely used BCIP/NBT reaction (Fig. 1A) or with the cerium technique (Fig. 1B). Both procedures result in similar staining intensities, suggesting comparable sensitivities of both procedures in enzyme cytochemistry.

Sensitivity is a problem when conventional cerium phosphate precipitation is intended for signal generation in alkaline phosphatase immunocytochemistry

Unfortunately, sensitivities were not at all comparable when both techniques were used for immunocytochemical purposes (see Discussion). This became evident when cell bodies and dendrites of dopaminergic periglomerular and tufted cells in the rat olfactory bulb were labeled with an antibody against tyrosine hydroxylase, followed by a biotinylated secondary antibody and alkaline phosphatase-labeled streptavidin. In these experiments, the conventional cerium phosphate technique hardly produced any staining (Fig. 1D). The BCIP/NBT method on the other hand yielded strong immunoenzymatic labeling of neuronal cell bodies and processes (Fig. 1C).

Therefore, when further attempting to use alkaline phosphatase as detection system in electron microscopic immunocytochemistry, the efforts had to be focused on substantially increasing the sensitivity of the conventional cerium procedure.

The sensitivity problem requires the development of an oCPP technique

To increase sensitivity and staining intensity we optimized the conventional cerium phosphate procedure. Various reaction parameters such as buffer systems, substrates, pH values, and cofactors had to be analyzed. As secondary antibodies and streptavidin for alkaline phosphatase-based immunocytochemistry usually contain the alkaline phosphatase from calf intestine, this isoform of the enzyme was used for the elaboration of the novel technique.

Possible substrates for immunocytochemistry include β-glycerophosphate, para-nitrophenyl phosphate, and ethanolamine phosphate. Whereas the latter produced a precipitate that was diffusely distributed over the sections (not shown), the two other phosphates resulted in a precisely localized precipitate that did not spread out from the site of antibody binding. For all subsequent experiments para-nitrophenyl phosphate was chosen as substrate. It allows the detection of alkaline phosphatase activity by cytochemical as well as by biochemical procedures.

Fig. 1A–D Comparison of bromochloroindolyl phosphate/nitro blue tetrazolium (BCIP/NBT) and conventional cerium phosphate for visualization of alkaline phosphatase activity in enzyme cytochemistry and immunocytochemistry. Endogenous alkaline phosphatase activity is visualized in the cortical tubule system of the rat kidney by enzyme cytochemistry (**A**, **B**). In this paradigm, the conventional cerium procedure (**B**) is as sensitive as the BCIP/NBT technique (**A**). In immunocytochemical labeling, however, differences in sensitivity are obvious (**C**, **D**). Dopaminergic neurons and fibers of periglomerular cells in the glomerula and tufted cells in the external plexiform layer of the rat olfactory bulb were labeled using a monoclonal antibody against tyrosine hydroxylase, biotinylated secondary antibodies, and alkaline phosphatase-labeled streptavidin as detection system. The BCIP/NBT method yielded strong immunoenzymatic labeling (**C**). In contrast, using the conventional cerium phosphate procedure only a few periglomerular cells were sparsely positive. Labeling of neuronal processes was completely absent (**D**). *ONL* Olfactory nerve layer, *GL* glomerular layer, *EPL* external plexiform layer, *MCL* mitral cell layer, *IPL* internal plexiform layer, *GRL* granule cell layer. *Bars* 500 µm in **A**, **B**; 200 µm in **C**, **D** ▶

Colorimetric determination of alkaline phosphatase activity was used to optimize the buffer system, pH value, and ionic composition of the incubation solution. The biochemical experiments (see Materials and methods) disclosed a tricine/diethanolamine mixture as the preferred buffer system, superior to simple tricine or glycine/tricine mixtures (Fig. 2A). Enzyme activity peaked at a pH value of 10.0 (not shown) and 3 mM cerium (Fig. 2B). Higher cerium concentrations tended to inhibit the enzyme. Magnesium sulfate increased the

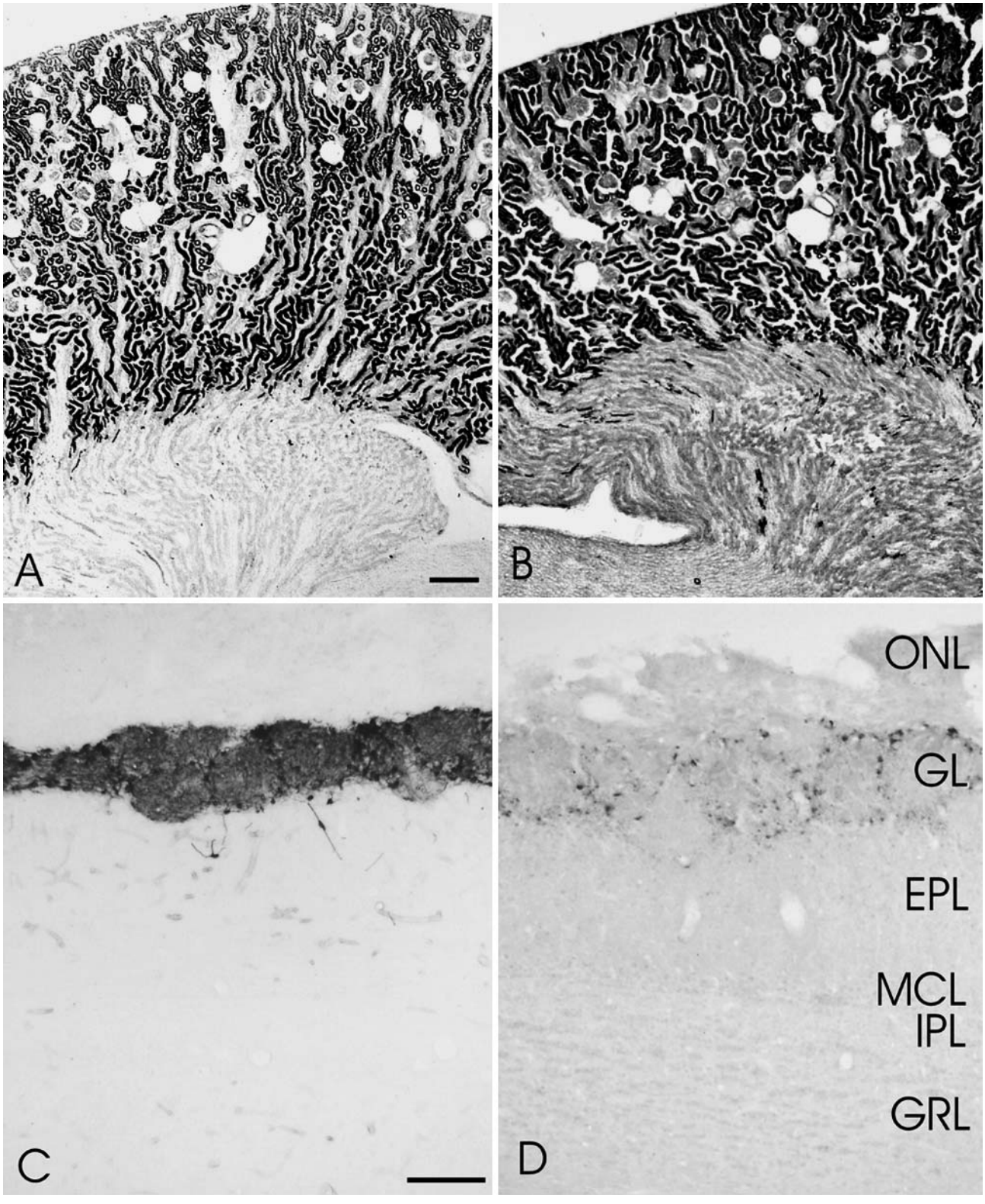

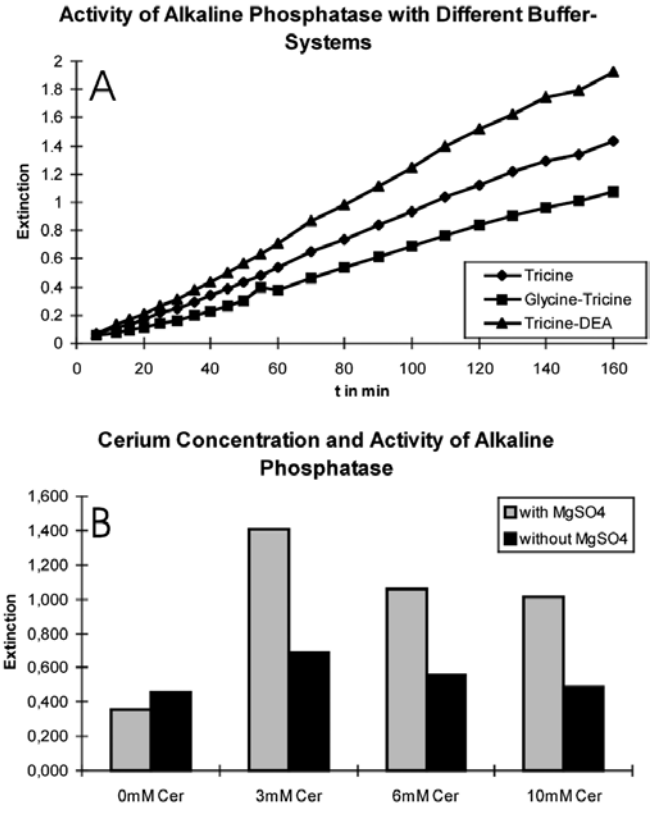

Fig. 2A, B Alkaline phosphatase activity in the presence of varying buffer systems and cerium concentrations. The influence of various buffer systems on the alkaline phosphatase reaction rate was investigated by photometric determination of the reaction product nitrophenol at 405 nm (**A**). Tricine/diethanolamine (*DEA*) accelerated the reaction in comparison with tricine or glycine/tricine buffers. Similarly, alkaline phosphatase activity was influenced by cerium concentration (**B**, *black bars*). In tricine/diethanolamine buffer, 3 mM cerium allowed the maximum reaction rate. The presence of magnesium sulfate in the buffer additionally accelerated the reaction (**B**, *gray bars*)

reaction rate (Fig. 2B), most likely through a positive allosteric effect of magnesium ions on the phosphatase molecule (Cappelet-Tordo et al. 1974; Bretaudiere and Spillman 1984).

Immunocytochemical experiments supported and extended the biochemical data. In keeping with the results of colorimetric experiments, immunolabeling at pH 10.0 was most intense. In buffers containing diethanolamine non-specific background staining was reduced and the reaction rate increased. Mixtures of 50 mM tricine and 50 mM diethanolamine provided the best results. Tricine concentrations above 50 mM reduced the sensitivity of the alkaline phosphatase reaction and an increased background staining. Finally, 30% sucrose in the incubation mixture (Halbhuber et al. 1994) improved distinct labeling of neuronal structures (data not shown).

The optimized and highly sensitive CPP procedure is subsequently called the oCPP technique. Its sensitivity as shown in the rat olfactory bulb (Fig. 3B) is now comparable to that of the BCIP/NBT procedure (Fig. 3A) and much higher than the conventional cerium phosphate procedure (Fig. 3C). In light microscopic single staining, some cracks in immunolabeled structures (Fig. 3B *arrows*) may be due to the fact that in this technique DAB is precipitated on top of the product of the oCPP reaction. This results in very rigid but fragile structures at the site of antibody binding. These problems are absent at the electron microscopic level.

The novel oCPP technique allows simultaneous immunoenzymatic double staining of two antigens at the light microscopic level

In the olfactory bulb tyrosine hydroxylase-positive dendrites of periglomerular cells are clearly labeled by the yellow oCPP product (Fig. 4A). Adjacent sections show serotoninergic fibers which target olfactory glomerula (Fig. 4B) and are visualized via the ABC technique. After double staining, the yellow cerium-(IV)-containing precipitate is clearly distinguished from the dark brown DAB reaction product (Fig. 4C). Obviously, the two visualization procedures are compatible for double labeling and do not interfere with each other.

At the ultrastructural level, peroxidase and alkaline phosphatase reaction products cannot be distinguished in a conventional transmission electron microscope

For the intended immunoenzymatic double labeling in electron microscopy, vibratome sections of the rat olfactory bulb were stained for tyrosine hydroxylase via the oCPP technique and for serotonin via the ABC procedure with DAB/osmium visualization. After flat embedding, light microscopic examination of semithin sections showed black serotoninergic axons (Fig. 5A *arrow*), while tyrosine hydroxylase-positive cell bodies (Fig. 5A *arrowhead*) were only slightly darker than adjacent negative ones.

At the ultrastructural level (Fig. 5B–D), serotoninergic fibers at low (Fig. 5B *arrows*) and high (Fig. 5C *asterisks*) magnifications as well as dopaminergic neurons (Fig. 5B *arrowhead*) contained electron-dense material. These precipitates could not be distinguished from each other by conventional electron microscopy.

Ultrastructural details are surprisingly well preserved (Fig. 5C, D), and astrocyte extensions (Fig. 5C) as well as presynaptic terminals with their vesicles and the postsynaptic densities (Fig. 5D) are easily recognized.

Energy-filtered transmission electron microscopy allows the specific visualization of cerium-containing precipitates

Differentiation of the precipitates was achieved by element-specific visualization of cerium via EFTEM. A

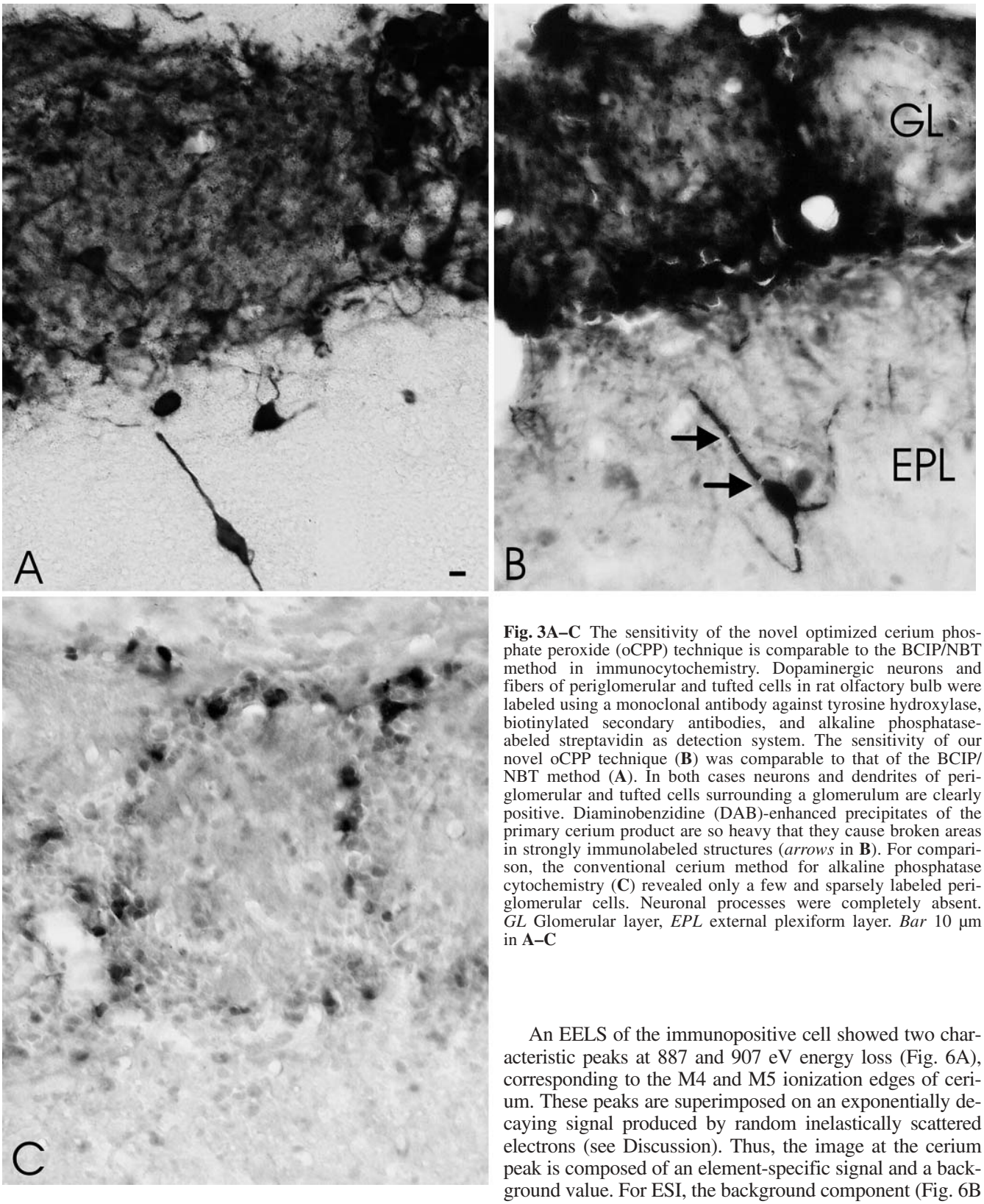

Fig. 3A–C The sensitivity of the novel optimized cerium phosphate peroxide (oCPP) technique is comparable to the BCIP/NBT method in immunocytochemistry. Dopaminergic neurons and fibers of periglomerular and tufted cells in rat olfactory bulb were labeled using a monoclonal antibody against tyrosine hydroxylase, biotinylated secondary antibodies, and alkaline phosphatase-abeled streptavidin as detection system. The sensitivity of our novel oCPP technique (**B**) was comparable to that of the BCIP/NBT method (**A**). In both cases neurons and dendrites of periglomerular and tufted cells surrounding a glomerulum are clearly positive. Diaminobenzidine (DAB)-enhanced precipitates of the primary cerium product are so heavy that they cause broken areas in strongly immunolabeled structures (*arrows* in **B**). For comparison, the conventional cerium method for alkaline phosphatase cytochemistry (**C**) revealed only a few and sparsely labeled periglomerular cells. Neuronal processes were completely absent. *GL* Glomerular layer, *EPL* external plexiform layer. *Bar* 10 μm in **A–C**

candidate cerium-labeled periglomerular neuron in the olfactory bulb (Fig. 5B *arrowhead*) and an immunolabeled fiber (Fig. 5B *arrows*) in the vicinity of a neighboring cell were selected for EFTEM analysis.

An EELS of the immunopositive cell showed two characteristic peaks at 887 and 907 eV energy loss (Fig. 6A), corresponding to the M4 and M5 ionization edges of cerium. These peaks are superimposed on an exponentially decaying signal produced by random inelastically scattered electrons (see Discussion). Thus, the image at the cerium peak is composed of an element-specific signal and a background value. For ESI, the background component (Fig. 6B *upper left*) is extrapolated pixel by pixel from two pre-edge images. Subtracting background values from the cerium edge signal (Fig. 6B *upper right*) according to the three-window power law method (Reimer et al. 1992) yields the specific cerium distribution image (Fig. 6B *lower right*).

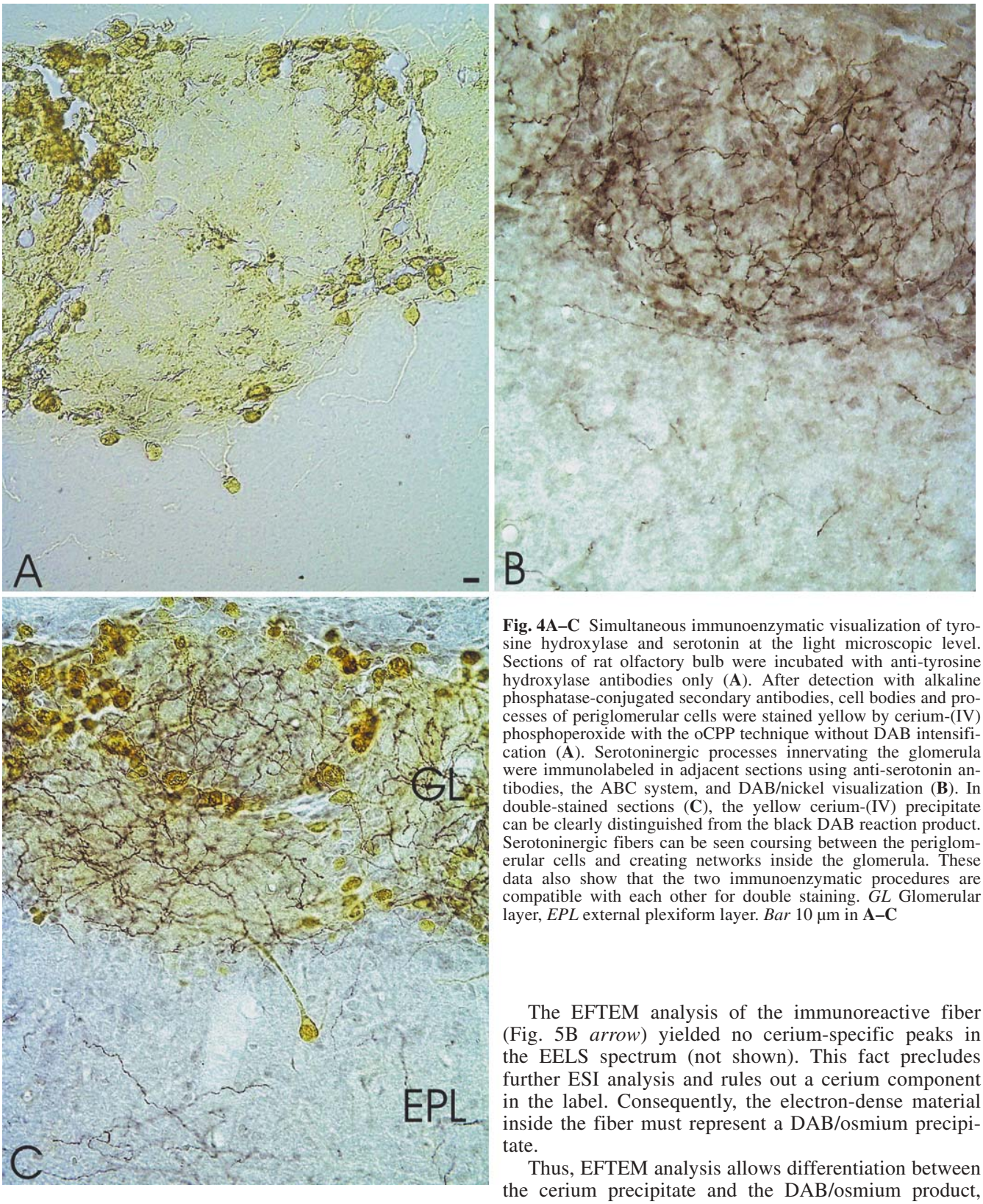

Fig. 4A–C Simultaneous immunoenzymatic visualization of tyrosine hydroxylase and serotonin at the light microscopic level. Sections of rat olfactory bulb were incubated with anti-tyrosine hydroxylase antibodies only (**A**). After detection with alkaline phosphatase-conjugated secondary antibodies, cell bodies and processes of periglomerular cells were stained yellow by cerium-(IV) phosphoperoxide with the oCPP technique without DAB intensification (**A**). Serotoninergic processes innervating the glomerula were immunolabeled in adjacent sections using anti-serotonin antibodies, the ABC system, and DAB/nickel visualization (**B**). In double-stained sections (**C**), the yellow cerium-(IV) precipitate can be clearly distinguished from the black DAB reaction product. Serotoninergic fibers can be seen coursing between the periglomerular cells and creating networks inside the glomerula. These data also show that the two immunoenzymatic procedures are compatible with each other for double staining. *GL* Glomerular layer, *EPL* external plexiform layer. *Bar* 10 μm in **A–C**

Ultrastructural localization of the precipitate is achieved when the specific cerium signal is superimposed on an inverted high-contrast electron micrograph (Fig. 6B *lower left*) taken at the carbon edge (energy loss of 250 eV).

The EFTEM analysis of the immunoreactive fiber (Fig. 5B *arrow*) yielded no cerium-specific peaks in the EELS spectrum (not shown). This fact precludes further ESI analysis and rules out a cerium component in the label. Consequently, the electron-dense material inside the fiber must represent a DAB/osmium precipitate.

Thus, EFTEM analysis allows differentiation between the cerium precipitate and the DAB/osmium product, thereby distinguishing tyrosine hydroxylase and serotonin immunoreactivities. An immunostained periglomerular cell (Fig. 5B *upper right corner*), therefore, is identified as dopaminergic due to high cerium content of the precipitate (Fig. 6C). In contrast, a darkly stained fiber

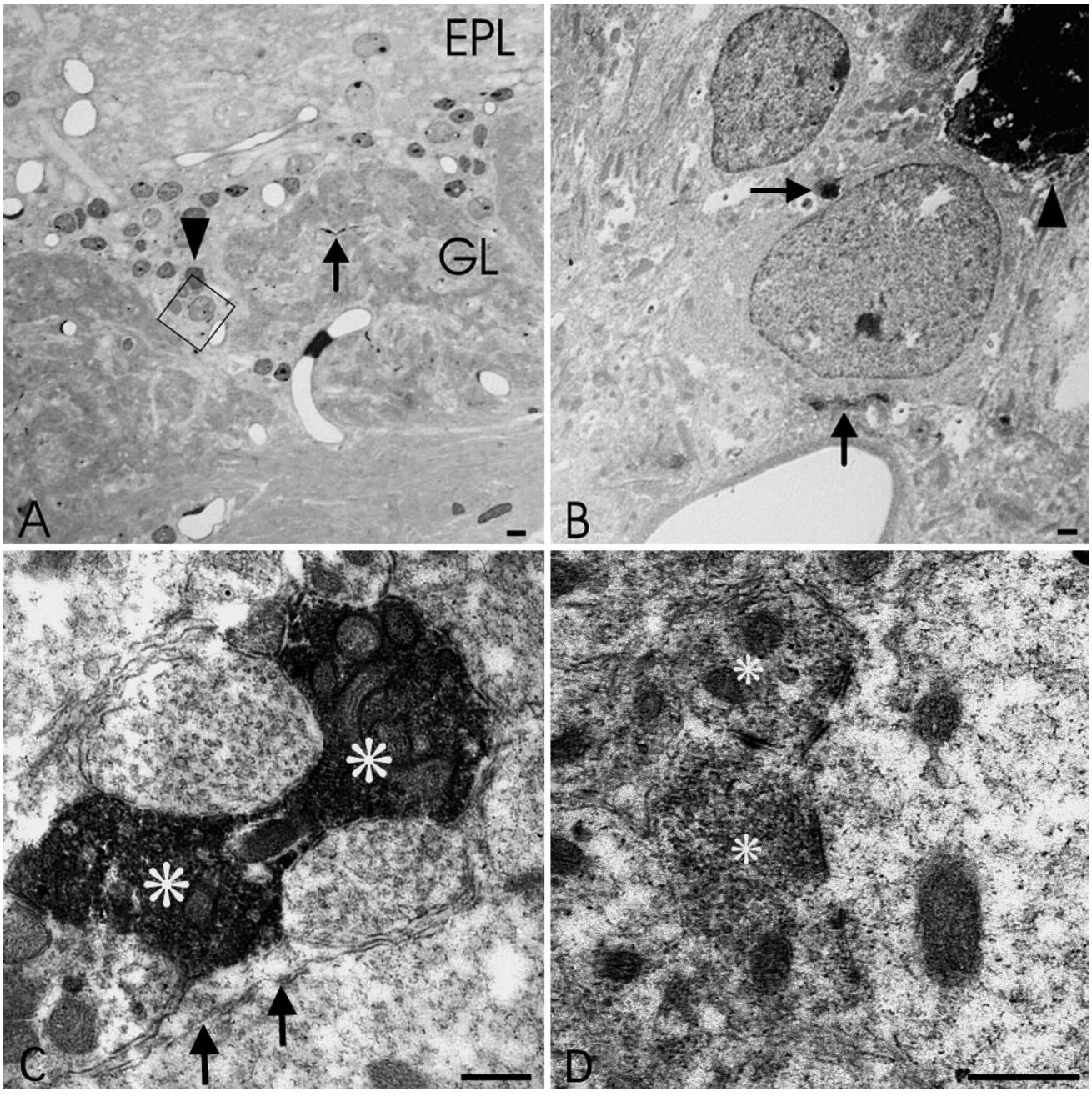

Fig. 5A–D Immunoenzymatic visualization of tyrosine hydroxylase and serotonin in rat olfactory bulb at the electron microscopic level. Vibratome sections of olfactory bulb were double stained for tyrosine hydroxylase and serotonin prior to embedding in Araldite. In the survey micrograph (**A**), the area of the electron micrograph (**B**) is *boxed*. At the ultrastructural level, the cerium (tyrosine hydroxylase, *arrowhead*) and DAB/osmium precipitates (serotonin, *arrows*) cannot be distinguished by conventional electron microscopy (**B**) because both are electron dense and yield a black label. Preservation of ultrastructure is acceptable as seen (**C**) from a tiny astrocyte extension (*arrows*) close to a serotoninergic axon profile [*asterisks*, no cerium in electron spectroscopic imaging (ESI)] and (**D**) from two immunonegative synaptic terminals (*asterisks*) on a large dendrite. *GL* Glomerular layer, *EPL* external plexiform layer. *Bars* 10 μm in **A**; 1 μm in **B**; 200 nm in **C**; 500 nm in **D**

(Fig. 5B *arrow*) shows no cerium (Fig. 6C *arrow*) and therefore represents a serotoninergic axon.

Energy-filtered transmission electron microscopy may allow to obtain quantitative data from immunocytochemical analysis

In some of the cerium-labeled, tyrosine hydroxylase-positive neurons, the immunoreactivity appeared to be more intense in neuronal processes than in the perikaryon (Fig. 7). This finding indicates that the oCPP technique may also be useful for the quantification of antigen concentrations at the ultrastructural level. However, the

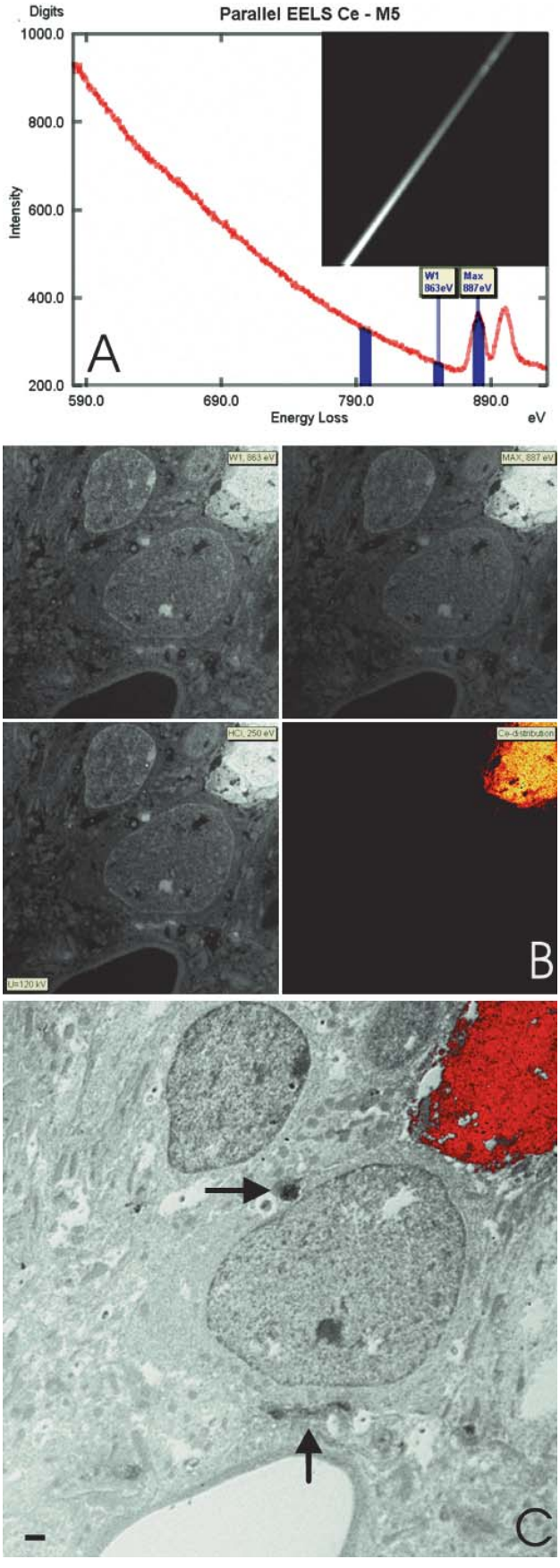

extensive calibrations required for quantification were beyond the scope of the present study.

Morphological analysis of serotonin-containing axons in the rat olfactory bulb

At the light microscopic level serotonin-positive axons with their typical beaded appearance were prominent in the glomerular layer of the olfactory bulb in single- (Fig. 4B) as well as in double-stained (Fig. 4C) sections. Corresponding areas in adjacent sections were screened in the electron microscope for the presence of presynaptic terminals on tyrosine hydroxylase-positive neurons.

Surprisingly, no serotoninergic synapses could be detected on dopaminergic neurons, when up to 60 serotonin-positive axon profiles in about ten ultrathin sections from several blocks were investigated. Subsequent screening for any serotoninergic synapses as identified by the presence of pre- and postsynaptic structures remained negative. This result was confirmed in about 20 serotonin-positive profiles in single-stained sections, where presynaptic vesicles but no postsynaptic specializations on adjacent neuronal somata or dendrites could be identified.

Fig. 6A–C Simultaneous immunoenzymatic visualization of tyrosine hydroxylase and serotonin in rat olfactory bulb at the electron microscopic level. The discrimination of cerium and DAB/osmium precipitates at the ultrastructural level is based on inelastic scattering (see Fig. 8) of beam electrons. Specific visualization of these electrons requires an energy-filtered transmission electron microscope like the LEO 912 Omega machine. Appropriate elements in the precipitates may be identified with the aid of an energy loss spectrum. For this purpose, an energy filter (omega filter) disperses the electrons along an axis (**A**, *inset*), depending on the energy (speed) at which they arrive. In the absence of special materials, low energy consuming interactions between the electron beam and the section occur at random. Consequently, plotting the number of electrons (current intensity) arriving at the screen versus their corresponding energy (electron energy loss spectrum, EELS) results in an exponential decay (**A**). When, however, the beam has passed a structure with a high density of cerium, many electrons have lost exactly the ionizing energies of M4 or M5 shell electrons, resulting in well-defined peaks in the electron energy loss spectrum (**A**, peaks at 887 and 907 eV). These peaks, therefore, identify the presence of cerium in the precipitate. A cerium-specific electron spectroscopic image (ESI; **B**, *lower right*) is obtained, when the image at the cerium peak at 887 eV (**B**, *upper right*) is corrected for background (**B**, *upper left*) with the three-window power law method (Beckers et al. 1996; Hendzel and Bazett-Jones 1996; Leapman et al. 1997; Martin et al. 1999; Akagi et al. 2000). Detailed morphological information is taken from a high-contrast image at 250 eV energy loss (**B**, *lower left*). For the final result (**C**), the specific cerium distribution (**B**, *lower right*) is superimposed in red color on the high-contrast image (**B**, *lower left*, inverted). Now the red cell in the *upper right corner* due to its cerium content is identified as a tyrosine hydroxylase-positive dopaminergic neuron, while the two dark fibers (*arrows*) do not contain cerium and thus represent serotoninergic axons (**C**). *Bar* 1 μm

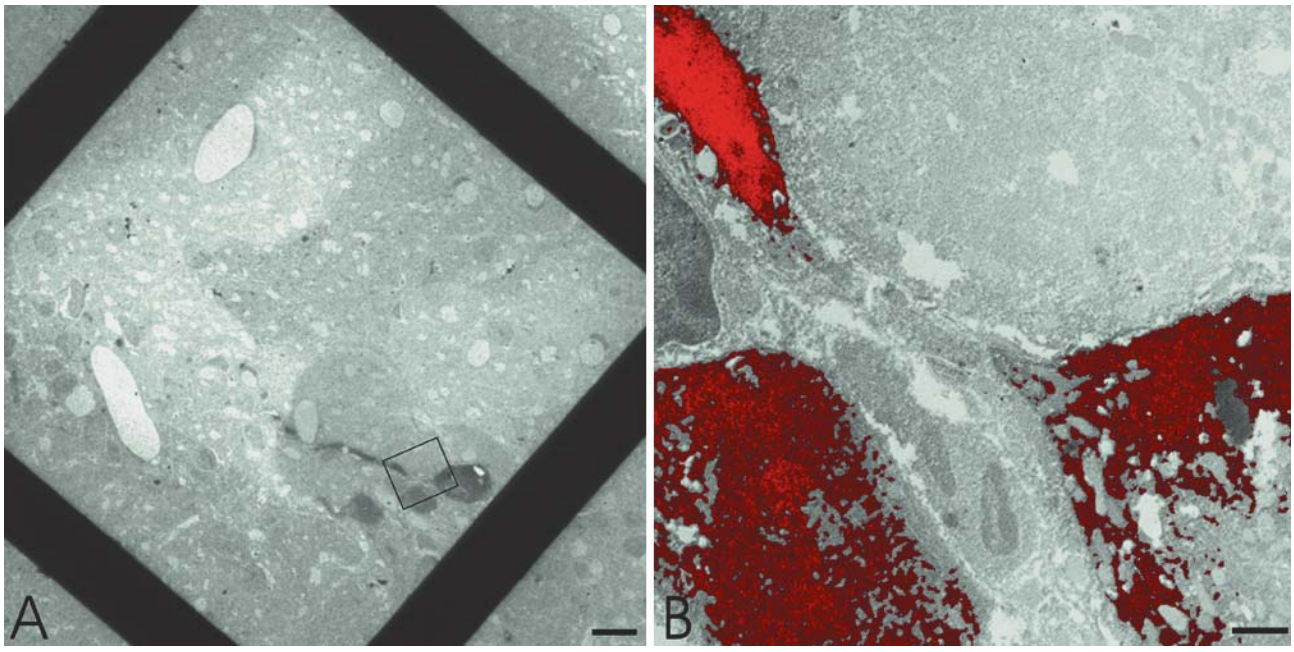

Fig. 7A, B Semiquantitative aspects of the oCPP technique in combination with energy-filtered transmission electron microscopy (EFTEM). Vibratome sections of rat olfactory bulb were immunostained for tyrosine hydroxylase and visualized by the novel oCPP technique. Subsequent to ultrathin sectioning, three tyrosine hydroxylase immunopositive periglomerular cells are shown in the survey electron micrograph (**A**). A large process of one of these cells is also labeled (*boxed area* in **A**, enlargement in **B**). At higher magnification (**B**), a pseudocolor image displaying the cerium distribution by ESI shows that immunoreactivity is more intense in the process (bright red) as compared to the perikaryon (darker red) of the neuron. However, antigen quantification at the electron microscopic level using the oCPP technique and ESI (EELS) will require further extensive calibrations. *Bar* 10 µm in **A**; 1 µm in **B**

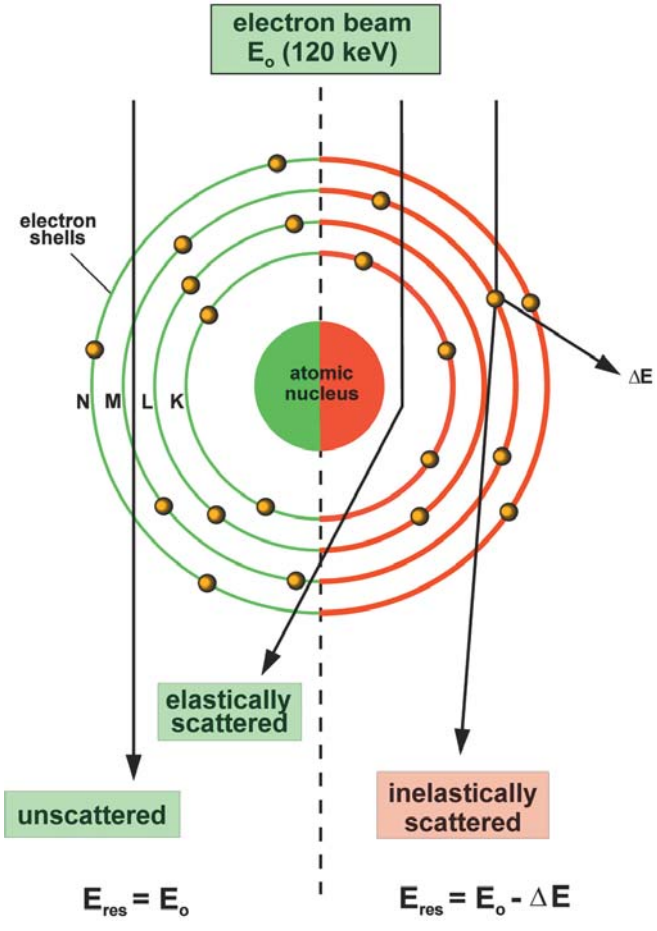

Discussion

The aim of the present study was to extend the use of alkaline phosphatase for immunoenzymatic double labeling from the light microscopic to the electron microscopic level.

Alkaline phosphatase-conjugated secondary antibodies or streptavidin are widely used in immunocytochemistry at the light microscopic level. In these cases, phosphatase activity is commonly visualized via the BCIP/NBT reaction. The corresponding precipitate, however, is soluble in ethanol and of low electron density, precluding its use at the ultrastructural level.

Fig. 8 Schematic representation of possible interactions of electrons of the beam with atoms of the section. In the electron microscope, beam electrons passing through the section may (brown, *right side*) or may not (green, *left side of scheme*) interact with atoms inside the section (scheme modified from Reimer et al. 1992). Elastic scattering at an atomic nucleus does not lead to energy loss. It simply changes the flight direction of the electron, which consecutively will not arrive at the screen. This phenomenon is the basis of contrast in conventional transmission electron microscopy. Some electrons of the beam, however, will hit other ones in the electron shells of atoms inside the section (inelastically scattered), resulting in ionization of the target atoms. After such an event, the original energy of the corresponding beam electron (E_0) is diminished by the ionization energy (ΔE) of the target electron, resulting in reduced kinetic energy (E_{res}) after having passed the section. These inelastically scattered electrons are used by EFTEM to identify and visualize the distribution of elements in the tissue. Lanthanides such as cerium are especially well suited for inelastic scattering (Reimer et al. 1992)

Table 1 Chemistry of the cerium-based alkaline phosphatase reaction (reaction sequence modified from Halbhuber et al. 1992)

1.	Alkaline phosphatase activity *p*-Nitrophenyl phosphate + $H_2O \rightarrow$ *p*-nitrophenol + PO_4^{3-}
2.	Cerium precipitation $xCe^{3+} + yPO^{3-}_4 + zOH^- \rightarrow$ Ce-(III)$_x$(OH)$_z$(PO$_4$)$_y$ Cerium precipitates with the phosphate released by the alkaline phosphatase and forms an invisible Ce(III) hydroxy phosphate
3.	Cerium oxidation and staining Ce(III)$_x$(OH)$_z$(PO$_4$)$_y$ + $nH_2O_2 \rightarrow$ Ce-(IV)$_x$(OH)$_{z-n}$(OOH)$_n$(PO$_4$)$_y$ + nH_2O The yellow Ce(IV) perhydroxy phosphate yields an alcohol insoluble and electron-dense reaction product
4.	Diaminobenzidine (DAB) enhancement (precipitation) Ce-(IV)$_x$(OH)$_{z-n}$(OOH)$_n$(PO$_4$)$_y$ + DAB $\rightarrow$ DAB (oxidized) The easily radicalizing Ce-(IV) perhydroxy phosphate oxidizes DAB. The resulting black precipitate stains the immunopositive regions providing good contrast for light microscopy

Visualization of alkaline phosphatase activity via the cerium phosphate procedure provides an ethanol insoluble, electron-dense precipitate

A second, well-established method for visualization of alkaline phosphatase activity is the cerium phosphate procedure. This method was originally developed for the cytochemical visualization of endogenous alkaline phosphatases in vertebrate tissues (Robinson and Karnovsky 1983; Halbhuber et al. 1992, 1994; van Noorden and Frederiks 1993). It takes advantage of the low solubility of cerium phosphate in aqueous solution. Inorganic phosphate is released by alkaline phosphatase activity from substrates such as para-nitrophenol. In the presence of cerium ions the free phosphate immediately precipitates as insoluble cerium-(III) phosphate. Subsequently, it is oxidized by hydrogen peroxide to the yellow and even less soluble cerium-(IV) peroxide phosphate (see Table 1). Application of this procedure, which provides an ethanol insoluble, electron-dense precipitate, to the immunocytochemical detection of antigens in tissue sections appeared straightforward.

The sensitivity of the conventional cerium phosphate procedure is not sufficient for immunocytochemical applications

To much of our surprise, however, the sensitivities of the BCIP/NBT reaction and the conventional cerium phosphate procedure, closely similar in the detection of endogenous enzyme activities (compare Fig. 1A and B), are strikingly different in immunoenzymatic applications (compare Fig. 1C and D). No straightforward explanations for this stunning fact are available at present. It might be due to kinetic differences between the two (rat kidney brush border versus calf intestine) isoenzymes.

Another possible reason could be that the solubility of the primary cerium phosphate precipitate is higher than that of the BCIP/NBT reaction product. If this was the case, the high local concentration of the phosphatase activity in the brush border of the kidney tubules would result in a high local concentration of liberated phosphate ions and in the immediate precipitation of cerium phosphate. In contrast, in immune complexes the local concentration of phosphatase activity will be much lower. Under these conditions, phosphate ions may be lost by diffusion, resulting in a lower steady state concentration of phosphate, which finally may preclude massive precipitation.

The above hypothesis is open to experimental verification. It requires the biochemical determination of relative phosphatase activities with respect to protein concentrations in both situations (endogenous versus immune-based activities). These experiments, however, were beyond the scope of the present investigation. Thus, the definitive reason for the low sensitivity of the conventional cerium phosphate procedure in immunocytochemical applications remains unclear at present.

Multiple labeling at the electron microscopic level is limited by the number of electron-dense signal systems available

Immunoelectron microscopic multiple staining procedures are limited in the number of markers to be visualized simultaneously in single tissue sections. For postembedding multiple staining, gold-labeled secondary antibodies or protein A are state of the art. The different immunocytochemical labels are distinguished by virtue of their size. Therefore, multiple labelings exceeding double labeling appear possible. However, increasing the size of colloidal gold particles results in a reduction of staining sensitivity. In practice, nanogold, 5- and 10-nm colloidal gold-labeled antibodies are used most frequently. Masking or destruction of antigens during the embedding procedure represents another problem. Embedding-sensitive epitopes are quite common, limiting the power of postembedding procedures in immunocytochemistry.

In preembedding techniques, peroxidase DAB and/or nanogold silver enhancement are used most commonly. Both colloidal metals and electron-dense immunoenzymatic precipitates result in a more or less black staining in electron micrographs. Metals can be differentiated, however, by their ultrastructural appearance and size. In contrast, enzymatic precipitates usually look similar, making a distinction of two different labels in the con-

ventional electron microscope impossible. In addition, artifacts formed during the staining procedure can occasionally not be distinguished from the immunolabeling. If specifically visualized, a cerium phosphate procedure with a substantially increased sensitivity, like the oCPP technique developed in the present report, should offer novel possibilities and add to available methods for multiple labeling at the electron microscopic level.

A cerium precipitate as product of the oCPP reaction can be specifically visualized by energy-filtered electron microscopy (EFTEM)

In an electron microscope, some electrons of the beam will specifically interact with other ones in the electron shells of the section material (Fig. 8, inelastically scattered). This type of interaction results in energy transfer (inelastic scattering) from the incoming electron to the molecules in the section. Lanthanides such as cerium are especially well suited for inelastic scattering (Reimer et al. 1992). If there is a high density of cerium in a defined structural element within a section, many electrons having passed this structure will arrive with reduced energy (speed) at the corresponding area of the screen. This effect, however, cannot be visualized in the conventional electron microscope.

In an energy-filtered transmission electron microscope like the LEO 912 Omega machine, however, an energy filter (omega filter) allows the selective visualization of those electrons which have lost energy when passing the section (for more detailed explanations see Figs. 6 and 8). With the aid of this filter, an element-specific, so-called electron spectroscopic image (ESI) is obtained (Fig. 6).

In our present investigation we have used this methodology to unequivocally differentiate cerium-containing precipitates, representing tyrosine hydroxylase-positive structures, from immunopositive but cerium-negative, serotoninergic axons in our sections at the electron microscopic level. The successful combination of EFTEM analysis with the highly sensitive oCPP method developed in the present investigation represents an important step toward the development of methods for simultaneously labeling four or more antigens in one single ultrathin section.

Additional candidate labels for EFTEM-based immunocytochemical visualization systems

Several conventional markers in electron microscopic immunocytochemistry such as immunogold (Haking et al. 1998) and silver (Radcke and Veh unpublished data) can be specifically detected by EFTEM. An additional label which has been used in EFTEM is boron conjugated to secondary antibodies or protein A (Bendayan et al. 1989; Qualmann et al. 1996). Europium (Takalo et al. 1994), gadolinium (Rebizak et al. 1997), iron as ferritin (Beckers et al. 1998), or dextran-covered iron oxide (Kresse et al. 1998; Radcke and Veh unpublished data) are other metals which are well suited for EELS and ESI and represent potential markers for EFTEM immunocytochemistry. Conceivably, the addition of these markers to the repertoire of immunocytochemical labels will even further extend the potential for simultaneous multiple labeling at the ultrastructural level.

The combination of the oCPP technique with the ABC method allows the simultaneous immunoenzymatic visualization of tyrosine hydroxylase and serotonin in the rat olfactory bulb at the ultrastructural level

As a result of the present investigation, the successful combination of the oCPP technique with the ABC method allows the simultaneous immunoenzymatic visualization of tyrosine hydroxylase and serotonin in the rat olfactory bulb. At the light microscopic level we found dense networks of serotoninergic fibers in the glomerular layer of the olfactory bulb. These results are in keeping with tract-tracing studies showing that the olfactory bulb receives significant ascending projections from the midbrain raphe nuclei (Moore et al. 1978; McLean and Shipley 1987; Araneda et al. 1989, 1999), which were identified as serotoninergic by immunocytochemical double labeling (McLean and Shipley 1987; Araneda et al. 1989, 1999). Some of the fibers were found in close proximity to dopaminergic periglomerular cells suggestive of formation of synaptic contacts.

At the electron microscopic level, however, we did not find synaptic contacts between serotoninergic fibers and dopaminergic periglomerular cells or their processes. So far, we were unable to find synaptic contacts with any neuronal element in the glomerular layer of the rat olfactory bulb. These findings would argue for a paracrine action of serotonin. A more systematic analysis of these axons is required, however, before conclusions about the olfactory bulb circuitry can be drawn.

With respect to the methodological focus of our study, the successful ultrastructural visualization of tyrosine hydroxylase-positive periglomerular cells via alkaline phosphatase immunocytochemistry shows that the combination of the present oCPP technique with EFTEM is a sensitive addition to the repertoire of immunoenzymatic labels for electron microscopy. It is compatible with the peroxidase/DAB reaction and, therefore, extends the possibilities for simultaneous multiple immunolabeling at the electron microscopic level.

Acknowledgements The work was supported by a grant from the Forschungskommission of the Charité (89452067). The authors are indebted to Dr. Mareike Wenzel for invaluable technical advice and fruitful discussions and to Dr. Angelika Görtzen for critically reading the manuscript. We wish to thank Heike Heilmann and Petra Loge for technical assistance, and Annett Kaphahn for secretarial help. The continuous advice and support from LEO Elektronenmikroskopie in Oberkochen is gratefully acknowledged.

References

Akagi T, Hashikawa T, Hirai K, Motelica-Heino I, Tsuji S (2000) Electron spectroscopic imaging (ESI) of cobalt ions responsible for the blockade of synaptic transmission and excitability of muscle cells in frog neuromuscular preparations. Proc Jpn Acad 76:7–11

Araneda S, Magoul R, Calas A (1989) Tracing specific transmitter pathways in the rat CNS: combination of [3H]serotonin retrograde labelling with immunocytochemical detection of endogenous transmitters. J Neurosci Methods 30:211–218

Araneda S, Gysling K, Calas A (1999) Raphe serotoninergic neurons projecting to the olfactory bulb contain galanin or somatostatin but not neurotensin. Brain Res Bull 49:209–214

Beckers AL, Gelsema ES, De Bruijn WC, Celton-Soeteman MI, Van Eijk HG (1996) Quantitative electron spectroscopic imaging in bio-medicine: evaluation and application. J Microsc 183:77–88

Beckers AL, De Bruijn WC, Jongkind JF, Celton-Soeteman MI, Apkarian RP, Gelsema ES (1998) Energy-filtering transmission electron microscopy as a tool for structural and compositional analysis of isolated ferritin particles. Scanning Microsc Suppl 8:261–275

Behringer DM, Meyer KH, Veh RW (1991) Antibodies against neuroactive amino acids and neuropeptides. II. Simultaneous immunoenzymatic double staining with labeled primary antibodies of the same species and a combination of the ABC method and the hapten-antihapten-bridge (HAB) technique. J Histochem Cytochem 39:761–770

Bendayan M, Barth RF, Gingras D, Londono I, Robinson PT, Alam F, Adams DM, Mattiazzi L (1989) Electron spectroscopic imaging for high-resolution immunocytochemistry: use of boronated protein A. J Histochem Cytochem 37:573–580

Bretaudiere JP, Spillman T (1984) Alkaline phosphatases. In: Bergmeyer HU, BergmeyerJ, Grassl M (eds) Methods of enzymatic analysis, vol IV. Enzymes 2: esterases, glycosidases, lyases, ligases. Chemie, Weinheim, pp 75–92

Cappelet-Tordo D, Fosset M, Iwatsubo M, Gache C, Lazdunski M (1974) Intestinal alkaline phosphatase. Catalytic properties and half of the sites reactivity. Biochemistry 13:1788–1795

Haking A, Troester H, Richter K, Burzlaff A, Spring H, Trendelenburg MF (1998) Heavy metal contrast enhancement for the selective detection of gold particles in electron microscopical sections using electron spectroscopic imaging. Bioimaging 6:130–137

Halbhuber KJ, Feuerstein H, Möller U, Klinger M (1992) Modified cerium-based and Gomori-based cerium methods for light microscopic phosphatase histochemistry: the cerium-perhydroxide-diaminobenzidine-nickel (Ce-H_2O_2-DAB-Ni and Ce/Ce-H_2O_2-DAB-Ni) two-step procedure. Acta Histochem 92:87–103

Halbhuber KJ, Schulze M, Rohde H, Bublitz R, Feuerstein H, Walter M, Linss W, Meyer HW, Horn A (1994) Is the brush border membrane of the intestinal mucosa a generator of "chymosomes"? Cell Mol Biol 40:1077–1096

Hendzel MJ, Bazett-Jones DP (1996) Probing nuclear ultrastructure by electron spectroscopic imaging. J Microsc 182:1–14

Kresse M, Wagener S, Pfefferer D, Lawaczeck R, Elste V, Semmler W (1998) Targeting of ultrasmall superparamagnetic iron oxide (USPIO) particles to tumor cells in vivo by using transferring receptor pathways. Magn Reson Med 40:236–242

Leapman RD, Gallant PE, Reese TS, Andrews SB (1997) Phosphorylation and subunit organization of axonal neurofilaments determined by scanning transmission electron microscopy. Proc Natl Acad Sci U S A 94:7820–7824

Martin R, Door R, Ziegler A, Warchol W, Hahn J, Breitig D (1999) Neurofilament phosphorylation and axon diameter in the squid giant fibre system. Neuroscience 88:327–336

McGadey J (1970) A tetrazolium method for non-specific alkaline phosphatase. Histochemie 23:180–184

McLean JH, Shipley MT (1987) Serotonergic afferents to the rat olfactory bulb. I. Origins and laminar specificity of serotonergic inputs in the adult rat. J Neurosci 7:3016–3028

Moore RY, Halaris AE, Jones BE (1978) Serotonin neurons of the midbrain raphe: ascending projections. J Comp Neurol 180:417–438

Noorden CJF van, Frederiks WM (1993) Cerium methods for light and electron microscopical histochemistry. J Microsc 171:3–16

Qualmann B, Kessels MM, Klobasa F, Jungblut PW, Sierralta WD (1996) Electron spectroscopic imaging of antigens by reaction with boronated antibodies. J Microsc 183:69–77

Rebizak R, Schaefer M, Dellacherie É (1997) Polymetric conjugates of Gd^{3+}-diethylenetriaminepentaacetic acid and dextran. 1. Synthesis, characterization, and paramagnetic properties. Bioconjug Chem 8:605–610

Reimer L, Zepke U, Moesch J, Schulze-Hillert ST, Ross-Messemer M, Probst W, Weimer E (1992) EEL spectroscopy. A reference handboock of standard data for identification and interpretation of electron energy loss spectra and for generation of electron spectroscopic images. Zeiss Electron Optics Division, Oberkochen

Reynolds ES (1963) The use of lead citrate at high pH as an electron-opaque stain in electron microscopy. J Cell Biol 17:208–212

Robinson JM, Karnovsky MJ (1983) Ultrastructural localisation of several phosphatases with cerium. J Histochem Cytochem 31:1197–1208

Takalo H, Mukkala VM, Mikola H, Liitti P, Hemmilä I (1994) Synthesis of europium(III) chelates suitable for labeling of bioactive molecules. Bioconjug Chem 5:278–282

Wenzel HJ, Buckmaster PS, Anderson NL, Wenzel ME, Schwartzkroin PA (1997) Ultrastructural localization of neurotransmitter immunoreactivity in mossy cell axons and their synaptic targets in the rat dentate gyrus. Hippocampus 7:559–570